

AD-A101 237

GENERAL ELECTRIC CO SYRACUSE N Y ELECTRONICS LAB  
HETERODYNING OPTICAL FIBER HYDROPHONE SYSTEM.(U)  
JUN 80 J L CHOVAN

F/6 17/1

UNCLASSIFIED

R80ELS-019

NL

A of 1  
401232

END  
DATE FILMED  
7-81  
DTIC

LEVEL

AD A1012317

DISTRIBUTION STATEMENT A  
Approved for public release;  
Distribution Unlimited

ELECTRONICS LABORATORY • SYRACUSE, N.Y.



276-111-100 series

12

AUTHOR J.L. Chovan	SUBJECT 210 Optical Principles and Devices	(14) X-100 R80ELS019
LEVEL HETERODYNING OPTICAL FIBER HYDROPHONE SYSTEM.		(11) DAY June 1980
		GE CLASS 1
REPRODUCIBLE COPY FILED AT TECHNICAL INFORMATION EP 3		GVT CLASS none
ELECTRONICS LABORATORY SYRACUSE, N.Y.		NO. OF PAGES 10
<p><b>SUMMARY</b> Optical fiber data transmission lines combined with acoustic sensors that directly modulate the light in the fibers offer the possibility of dramatic reductions in the size, weight, and cost of low frequency sonar sensor arrays. A practical problem in such systems is distinguishing the desired modulation imposed at the sensor location from undesired extraneous modulations accumulated along the entire fiber lead length. A system is presented which solves this problem. It uses a pair of single-mode optical fibers connected to each sensor. The boundaries between the sensing element and the fiber leads are delineated by partially reflecting optical discontinuities. The sensing element can be any device capable of optically coupling the two fibers together with an optical transit time delay that is affected by acoustic vibrations. An acoustically driven gap between the planar end faces of the two lead fibers, and a coiled optical fiber are examples of two suitable sensors that have been experimentally demonstrated in this system.</p> <p>Optical heterodyning techniques are used to obtain a phase modulated IF signal out of each fiber. The phase difference between these two channels represents the acoustic signal at the sensor, independently of lead length effects.</p> <p>Experimental data is presented along with a detailed analysis of the system.</p>		
KEY WORDS Optical Hydrophone, Optical Fibers, Optical Heterodyning, Acoustic Sensors, Sonar		

12 13

12

JUL 10 1980

INFORMATION PREPARED FOR UEPD

WORK CONDUCTED BY Author

APPROVED

SS MGR

SECT MGR

DISTRIBUTION STATEMENT A  
Approved for public release;  
Distribution Unlimited

141591

JF

## HETERODYNING OPTICAL FIBER HYDROPHONE SYSTEM

### Abstract

Optical fiber data transmission lines, combined with acoustic sensors that directly modulate the return light in the fibers, promise a significant reduction in size, weight, and cost of future sonar sensor arrays. Unfortunately, acoustic signals and mechanically induced strains also act along the entire lead length of the optical fiber to modulate the phase, intensity, and polarization of the light in the fiber. For long lead lengths, these undesirable effects can dominate over the signal modulation at the sensor site. This paper describes a system that is immune to such modulations induced along the lead lengths.

It uses a pair of single-mode optical fibers connected to each sensing element. The boundaries between the fibers and the sensing element are delineated by discontinuities which cause partial optical reflections. The sensing element can be any device capable of coupling light between the two fibers with an acoustically produced perturbation in the optical transit time between the boundaries. A coiled optical fiber, vibrating optical cavity, and a variable gap between the end faces of optical fibers are examples of suitable sensors.

Each fiber is fed with coherent light at slightly different optical frequencies, derived by seradyning a portion of a laser beam with an acousto-optic Bragg modulator. At the sensing element boundaries the return light in each fiber has a reflected component and a component transmitted through the sensing cell. Since these two components are at slightly different optical frequencies, the net intensity of the return light fluctuates at the IF difference frequency. The phase relationship between the reflected light and the transmitted light is modulated by the acoustic perturbations of the optical transit time through the sensor. Thus, the IF intensity of the return light in each fiber is phase modulated by the acoustic signal at the sensor.

Separate photodetectors are used to sense this IF signal returning from each fiber. It is shown that the phase difference between these two IF signals is modulated only by the signal at the sensor and not by any lead length modulation. It is not necessary for the undesirable lead length modulations in the two fibers to be similar to realize this cancellation.

Experimental results are also presented.

### Introduction

Figure 1 schematically illustrates the total system. A laser output at optical radian frequency  $\omega_0$  is passed through an acousto-optic Bragg modulator driven at frequency  $\omega$ . The drive amplitude is such that the first diffracted order at frequency  $\omega_0 + \omega$  is nominally equal in intensity to the undiffracted zero order at frequency  $\omega_0$ .

Each of these two orders pass through separate beamsplitting mirrors which act as directional couplers to isolate input light into the fiber from return light out of the fiber. Suitable optics are used to couple these two inputs to their respective single-mode fibers. Index matching cells are used to eliminate partial optical reflections from the fiber input faces.

The fibers conduct the light to the sensor boundaries. Ideally, the two fiber lengths are equal. The following analysis shows that exact matching is not critical.

At the sensor boundaries partial optical reflection occurs, with the reflected light returning along its original fiber. A portion of the transmitted light traverses the sensing element and enters the other fiber. Since the fibers are single mode, the optical wavefronts are uniform plane waves across the core and travel axially along the fiber. Thus, the wavefronts of both the reflected and the transmitted wave returning in a given fiber are congruent. This results in uniform optical interference over the cross-section of the fiber core. Since the reflected and transmitted waves differ in optical frequency by  $\omega$ , they are alternately in phase with constructive interference and out of phase with destructive interference. This results in the

return optical intensity fluctuating at the IF frequency  $\omega$ . The phase of this IF signal depends on the phase relationship between the reflected and transmitted components. Since this phase relationship depends on the optical transit through the sensing element, which is perturbed by the acoustic vibrations, the IF signal is phase modulated by the acoustic signal.

For discussion purposes the sensing element is assumed to be optically very lossy so that subsequent reflections back and forth within the sensor between the boundaries are negligible. Analysis shows that such multiple reflections result in a non-linear relationship between the acoustically induced path length changes and the corresponding IF phase modulations. Thus, a compromise is required between an optically lossy sensor which has low distortion and an optically efficient sensor which has good noise performance. Experimental results have demonstrated adequate sensitivity without objectionable distortion.

The light returning out of each fiber passes through the coupling optics and is reflected from the beamsplitting mirrors to the respective photodetectors. After suitable IF amplification, the phase difference between the two channels indicates the acoustically induced optical path length modulation at the sensor independently of any lead length effects.

#### System Analysis

For simplicity, laser coherence effects and polarization effects are neglected in the following analysis. It is assumed that the amplitude and phase of the light at any point in the system, suitably integrated over the entire cross-section of the beam, can be described as a complex number. The magnitude is in units of square root of power.

As long as the optical path length through the sensing cell, and the differential path lengths between the two legs from the Bragg modulator beam splitter through the fibers to the sensor boundaries are small compared to the coherence length of the laser, the analysis applies. Otherwise, a more general treatment is required which considers the cross correlation functions of the various optical components with suitable time delays at various points in the system.

Polarization can be decomposed into two orthogonal components with the analysis applying separately to each component.

Figure 2 identifies the nomenclature for the complex light amplitudes travelling toward and away from the sensor boundaries on both the fiber side and the sensor side of the boundaries. At a given boundary, the reflected components are related to the incident components by a scattering matrix as follows. In general, all terms are complex.

$$\begin{Bmatrix} B_1 \\ V_1 \end{Bmatrix} = \begin{bmatrix} S_{11} & S_{12} \\ S_{21} & S_{22} \end{bmatrix} \begin{Bmatrix} A_1 \\ U_1 \end{Bmatrix} \quad (1)$$

For no dissipative losses at the boundary, reciprocity and conservation of energy can be used to derive the following constraints on the elements of the scattering matrix [1].

$$S_{12} = S_{21} \quad (2a)$$

$$|S_{11}|^2 = |S_{22}|^2 = R = \text{power reflectivity} \quad (2b)$$

$$|S_{12}|^2 = 1-R = T = \text{power transmission} \quad (2c)$$

$$2\phi_{12} = \phi_{11} + \phi_{22} \pm \pi \quad (2d)$$

where

$$S_{mn} = |S_{mn}| \exp(\phi_{mn}).$$

Due to the extremely small cross-sectional area of the fiber core, even modest optical powers have very high power densities. If the boundaries were lossy and dissipated any appreciable fraction of the power,

these high densities would probably result in thermal damage. Thus, practical beamsplitting boundaries are likely to be limited to the lossless case as analyzed, due to thermal constraints.

The sensing cell can be characterized by an optical power transmission efficiency  $\xi$  (excluding boundary reflection effects) and an optical transit delay  $\tau$ , which is modulated by the acoustic signal of interest. This transit delay is converted to an optical phase shift  $\omega_0 \tau$ , where  $\omega_0$  is the optical radian frequency. It is assumed that  $\omega \tau$  is negligible, where  $\omega$  is the radian frequency shift introduced by the Bragg modulator. Using these definitions and those of Figure 2, the following relationships are evident:

$$U_1 = V_2 \sqrt{\xi} e^{-j \omega_0 \tau} \quad (3a)$$

$$U_2 = V_1 \sqrt{\xi} e^{-j \omega_0 \tau}. \quad (3b)$$

A matrix equation similar to that of Equation (1) also applies for boundary 2. Identical boundaries are assumed so that the elements of the scattering matrix  $S$  are the same in both cases. Those two matrix equations, along with Equations (3a) and (3b), result in six simultaneous equations. The six unknowns are  $B$ ,  $U$ , and  $V$  at each boundary. Algebraic manipulation of these equations to eliminate  $U$  and  $V$  for each boundary results in the following pair of simultaneous equations.

$$\begin{aligned} B_1 &= \left[ S_{11} + \frac{\xi S_{12} S_{21} S_{22} e^{-j 2 \omega_0 \tau}}{1 - \xi S_{22}^2 e^{-j 2 \omega_0 \tau}} \right] A_1 \\ &\quad + \left[ \frac{\sqrt{\xi} S_{12} S_{21} e^{-j \omega_0 \tau}}{1 - \xi S_{22}^2 e^{-j 2 \omega_0 \tau}} \right] A_2 \quad (4a) \\ B_2 &= \left[ \frac{\sqrt{\xi} S_{12} S_{21} e^{-j \omega_0 \tau}}{1 - \xi S_{22}^2 e^{-j 2 \omega_0 \tau}} \right] A_1 \\ &\quad + \left[ S_{11} + \frac{\xi S_{12} S_{21} S_{22} e^{-j 2 \omega_0 \tau}}{1 - \xi S_{22}^2 e^{-j 2 \omega_0 \tau}} \right] A_2. \end{aligned}$$

For convenience, the following definitions are made:

$$G = g e^{j \phi_g} = \left[ S_{11} + \frac{\xi S_{12} S_{21} S_{22} e^{-j 2 \omega_0 \tau}}{1 - \xi S_{22}^2 e^{-j 2 \omega_0 \tau}} \right] \quad (5a)$$

$$K = k e^{j \phi_k} = \left[ \frac{\sqrt{\xi} S_{12} S_{21} e^{-j \omega_0 \tau}}{1 - \xi S_{22}^2 e^{-j \omega_0 \tau}} \right] \quad (5b)$$

$$A_1 = \sqrt{P_1} e^{j (\omega_0 t + \theta_1)} \quad (5c)$$

$$A_2 = \sqrt{P_2} e^{j [(\omega_0 + \omega)t + \theta_2]}. \quad (5d)$$

where  $P_1$  and  $P_2$  are the optical powers incident on boundaries 1 and 2, and  $\theta_1$  and  $\theta_2$  are arbitrary time varying phases due to undesired lead length modulations.

Using these definitions in Equation (4) and multiplying by complex conjugates to obtain return powers at the boundaries, yield the following:

Accession For	
NTIS GRA&I	<input type="checkbox"/>
DTIC TAB	<input type="checkbox"/>
Unannounced	<input type="checkbox"/>
Justification	
By _____	
Distribution/	
Availability Codes	
All and/or	
Part	Special

(4a)

(4b)

(5a)

(5b)

(5c)

(5d)

$$|B_1|^2 = \left[ g^2 P_1 + k^2 P_2 \right] + 2 g k \sqrt{P_1 P_2} \cos \left[ \omega t + (\theta_2 - \theta_1) + (\phi_k - \phi_g) \right] \quad (6a)$$

$$|B_2|^2 = \left[ k^2 P_1 + g^2 P_2 \right] + 2 g k \sqrt{P_1 P_2} \cos \left[ \omega t + (\theta_2 - \theta_1) - (\phi_k - \phi_g) \right] \quad (6b)$$

Notice that these return powers contain a DC term and an AC term at the IF frequency  $\omega$ . The DC term contributes to shot noise, which sets an ultimate limit on the acoustic sensitivity. This is discussed in more detail in a later section.

The phase of the IF term contains the signal modulation in the  $\phi_k - \phi_g$  term. Notice from Equations (5a) and (5b) that for small  $\xi$  this phase difference is approximately  $(2\phi_{12} - \phi_{11} - \omega_0 \tau)$ . Thus, the phase is linearly related to  $\tau$ , the optical transit time through the sensing element, which is acoustically modulated. For larger values of  $\xi$ , the optical coupling efficiency through the sensor, a non-linear relationship exists between  $\tau$  and the phase modulation. This is discussed further in a later section.

Notice that in either fiber 1 or 2 the phase of the IF term is corrupted by the undesirable lead length phase modulations  $\theta_1$  and  $\theta_2$ . However, the phase difference between these two channels is  $2(\phi_k - \phi_g)$ , which is the desired signal and is independent of the lead length phase terms.

If a differential transit time exists between the two channels in returning from the sensor through the fibers and photodetectors and electronic circuitry to the phase detector, the cancellation of the phase noise  $\theta_1$  and  $\theta_2$  can be less than perfect. This is discussed further in the following section.

#### Lead Noise Cancellation

As mentioned earlier, the environment can induce intensity, polarization, and phase modulations along the fiber lead lengths to the sensor. The intensity and polarization modulations effect the powers  $P_1$  and  $P_2$  incident at the sensor boundaries. As seen from Equation (6), fluctuations in these terms effect only the amplitude but not the phase of the IF signals. Thus, they have no direct effect on the final output.

Conceptually, polarization shifts are potentially capable of causing orthogonal polarizations between  $P_1$  and  $P_2$ , thereby causing occasional fades in the IF signal as  $P_1 P_2$  approaches zero. Experimentally, such fading was not a problem.

On the other hand, the lead length phase modulations  $\theta_1$  and  $\theta_2$  directly affect the IF phase in each channel. The degree to which they can be cancelled at the phase detector depends on their time registration at the detector.

Due to an accumulation of differential fiber lengths and circuit propagation delay unbalances caused by tolerances, consider the two IF signals at the phase detector to be misregistered by a time  $\epsilon$ . The output phase difference  $\Delta$  is obtained from Equation (6), with the indicated time shift.

$$\begin{aligned} \Delta = & \left\{ \omega(t - \frac{\epsilon}{2}) + [\theta_2(t - \frac{\epsilon}{2}) - \theta_1(t - \frac{\epsilon}{2})] - [\phi_k(t - \frac{\epsilon}{2}) - \phi_g(t - \frac{\epsilon}{2})] \right\} \\ & - \left\{ \omega(t + \frac{\epsilon}{2}) + [\theta_2(t + \frac{\epsilon}{2}) - \theta_1(t + \frac{\epsilon}{2})] + [\phi_k(t + \frac{\epsilon}{2}) - \phi_g(t + \frac{\epsilon}{2})] \right\} \end{aligned} \quad (7)$$

It is enlightening to consider the frequency spectrum of this output signal. The signal and noise spectrums,  $Q_s$  and  $Q_n$ , are defined as follows for the single-channel phase terms.

$$Q_s(f) = \int_{-\infty}^{\infty} [\phi_g(t) - \phi_k(t)] e^{j2\pi ft} dt \quad (8a)$$

$$Q_n(f) = \int_{-\infty}^{\infty} [\theta_2(t) - \theta_1(t)] e^{j2\pi ft} dt \quad (8b)$$

The corresponding output signal and noise spectrum,  $Q_{so}$  and  $Q_{no}$ , are obtained by transforming the appropriate terms from Equation (7).

$$Q_{so}(f) = [e^{j\pi f\epsilon} + e^{-j\pi f\epsilon}] Q_s(f) = Q_s(f) 2 \cos(\pi f\epsilon) \quad (9a)$$

$$Q_{no}(f) = [e^{j\pi f\epsilon} - e^{-j\pi f\epsilon}] Q_n(f) = Q_n(f) 2 j \sin(\pi f\epsilon). \quad (9b)$$

As a practical matter, it should be easy to match fiber lead length differences to less than 10 cm, which implies  $\epsilon$  less than half a nanosecond. At 1 kHz acoustic modulation frequency, the above results imply about 116 dB suppression of the lead length noise with negligible effect on the signal. Furthermore, this suppression improves at 20 dB per decade with decreasing frequency or decreasing path length mismatch. Thus, it is realistic to expect significant lead noise suppression with practical tolerances.

#### Distortion

The final signal of interest was seen from Equations (7) and (9) to be  $2(\phi_g - \phi_k)$ . Combining Equations (5) and (2) leads to the following:

$$G = \frac{[1 - \xi e^{j2(\phi_{22} - \omega_0 \tau)}] \sqrt{R} e^{j\phi_{11}}}{1 - \xi R e^{j2(\phi_{22} - \omega_0 \tau)}} \quad (10a)$$

$$K = \frac{\sqrt{\xi} T e^{j(2\phi_{12} - \omega_0 \tau)}}{1 - \xi R e^{j2(\phi_{22} - \omega_0 \tau)}} \quad (10b)$$

The difference in phase angles between these two complex terms is determined.

$$2(\phi_g - \phi_k) = 2(\omega_0 \tau - \phi_{22}) + 2 \tan^{-1} \left\{ \frac{\xi \sin[2(\omega_0 \tau - \phi_{22})]}{1 - \xi \cos[2(\omega_0 \tau - \phi_{22})]} \right\} \quad (11)$$

Ideally, only the first term would exist yielding a linear relationship between the modulated term  $\tau$  and the measured output phase. The inverse tangent term contributes an undesirable non-linearity. For small optical efficiencies  $\xi$ , the non-linear addition is seen to approximately vary sinusoidally with  $\tau$ , having peak excursions of  $\xi$ . A plot of Equation (11) is shown in Figure 3. If linearity is not a severe requirement, values of  $\xi$  up to about 0.5 can probably be used. This is especially true if some form of electronic compensation is incorporated to correct for the non-linearity. As  $\xi$  approaches one, the slope of the input versus output curve is seen to get too small to be useful. For  $\xi$  below about 0.1, linearity is probably acceptable for most applications. Thus, it is desirable to use an optically inefficient sensing element maintaining a low  $\xi$  to limit non-linearities in the transfer function. Experimental results demonstrated acceptable sensitivity without noticeable distortion with an  $\xi$  of about 5 percent.

#### Photon Noise Limited Sensitivity

The optical power returning toward each photodetector is given by Equation (6). Multiplying this by some power transmission factor  $\gamma$ , which accounts for fiber losses and optical coupling losses from the fiber to the photodetector yields the power at the detector. Dividing this by the energy per photon,  $hc/\lambda$ , yields the number of photons per unit time at the detector. ( $h$  = Planck's constant,  $c$  = speed of light,  $\lambda$  = free space wavelength of the light.) Multiplying this photon rate by the quantum efficiency  $\eta$  of the detector results in the number of conduction electrons per unit time in the detector. Multiplying this by the charge per electron,  $e$ , yields the photo-induced detector current,  $i$ .

$$i = \frac{\gamma \lambda \eta e}{hc} |B|^2 \quad (12)$$

The average current in the photodetector is obtained from the DC term in Equation (6). Assuming the powers in fibers 1 and 2 are nominally equal and given by  $P$  leads to the following DC current  $i_0$ .

$$i_0 = \frac{\gamma \lambda \eta e P (g^2 + k^2)}{h c} \quad (13)$$

Due to the discrete nature of the photon generated conduction charges and the statistical fluctuation in their generation times, this average current is composed of a string of impulses having a white noise spectrum. The mean squared noise current,  $i_n^2$ , in a bandwidth  $B$  is given as follows:

$$i_n^2 = 2 e B i_0 \quad (14)$$

This is a fundamental photon noise floor which may be approached by mitigating all other noise sources, but cannot be eliminated.

The signal current,  $i_s$ , is obtained from the AC component of Equation (6):

$$i_s = \frac{\gamma \lambda \eta e 2 g k P}{h c} \quad (15)$$

The signal power out of the photodetector is proportional to the signal current squared. The noise power is proportional to the mean squared noise current given by Equation (14). This results in the following signal-to-noise ratio,  $\xi$ , which is the maximum achievable.

$$\xi = \frac{\gamma \lambda \eta 2 P}{h c B} \left( \frac{g^2 k^2}{g^2 + k^2} \right) \quad (16)$$

It is evident from Equation (10) that for small  $\xi$ ,  $g^2$  is approximately  $R$  and  $k^2$  is approximately  $\xi T^2$ .

$$\frac{g^2 k^2}{g^2 + k^2} \approx \frac{\xi R (1 - R)^2}{R + \xi (1 - R)^2} \quad \text{if } \xi \ll 1 \quad (17)$$

The factor is plotted in Figure 4.

It is evident from the plot that the optimum reflectivity generally ranges from about 5 percent to 25 percent depending on  $\xi$ . It is also evident that signal-to-noise ratio improves with increasing  $\xi$ . However, as  $\xi$  approaches unity, non-linearities occur as shown in Figure 3. Furthermore, for large  $\xi$  the approximation shown in Equation (17) is no longer valid. Exact analysis using Equation (10) shows that this factor becomes dependent on the transit time  $\tau$  through the sensor. In fact, particular values of  $\tau$  can seriously reduce the signal-to-noise ratio for values of  $\xi$  near one. Thus, cyclic signal fading can occur as  $\tau$  drifts with temperature or pressure if  $\xi$  is too large.

The ultimate minimum phase modulation that can be detected by this system is limited by the additive photon noise. Figure 5 illustrates a phasor diagram. The signal phase has a length equal to the square root of signal power and its phase angle is of interest. The noise phasor has a length equal to the square root of noise power and its phase angle is unknown. For large signal-to-noise ratio, it is evident from the figure that the RMS uncertainty in phase angle is the inverse of the square root of the signal-to-noise ratio.

The measured output phase  $\Delta$  is the difference between two IF phasors, each of which is corrupted by independent additive photon noise in the two channels. Thus, the net RMS phase uncertainty  $\delta$  is the square root of two larger than that of a single channel.

$$\delta = \sqrt{2/\xi} \quad (18)$$

As a representative bench mark, consider 1 milliwatt of laser power in each fiber incident at the sensor, a 10 percent transmission efficiency back to the detector, and 0.05 for the factor plotted in Figure 4. This corresponds to 5 microwatts returned to each detector. Assuming a helium neon laser with a wavelength of 0.6328 microns and a photodetector quantum efficiency of 0.35 results in a signal-to-noise ratio, from Equation (16) of about 130 dB normalized to a 1 Hz bandwidth. This corresponds to an output RMS phase noise of about  $4 \times 10^{-7}$  radians in a 1 Hz bandwidth. Under these conditions the acousto-optic properties of the sensing cell would have to produce phase modulations, given essentially by  $\omega_0 \Delta \tau$ , which are

large compared to this. ( $\Delta \tau$  = RMS transit time modulation acoustically produced in sensor in a 1 Hz bandwidth.)

### Experimental Results

A sensor which was used in the experimental system is schematically shown in Figure 6. It consists of a thin-walled brass cylinder about 2 cm long and 1 cm in diameter. Its ends are sealed with compliant rubber diaphragms which, along with internal diaphragms as shown, support the ends of single-mode optical fibers. The fibers are axially aligned with a gap of a few mils between the cleaved end faces. The cell is air filled.

The gap between the fibers is the heart of the sensor. Its boundaries are the glass-to-air interfaces at the fiber ends, which produce about 4 percent reflection due to the optical index change. Light exits the fiber in an expanding cone, with a small portion being coupled into the opposite fiber. The gap was such that this coupled portion was comparable to the reflected light.

Sound, which is a pressure fluctuation at an acoustic rate, deflects the diaphragms to equalize the internal and external pressures. This diaphragm vibration drives the fibers axially, thereby modulating the gap length and corresponding optical transit time through the gap.

Figure 7a shows a typical IF spectrum before demodulation. It was obtained by mixing the two photodetector outputs with slightly different frequencies, thus obtaining offset IF signals. These two offset signals were then mixed with each other to obtain the difference frequency shown in the figure. This process results in an IF signal modulated by the difference in phases between the two photodetector signals.

The scale in the figure is 0 to 20 kHz horizontally and 10 dB/cm vertically. As seen in the data, the modulation sideband is 34 dB down from the carrier. The carrier and first order sidebands are respectively proportional to the zero and first order Bessel functions having arguments equal to the peak phase deviation induced by the modulation. This corresponds to about 0.04 radians peak phase deviation which implies about 14 Angstroms RMS vibration of the gap.

Figure 7b shows this same signal after phase demodulation. The scale is 0 to 2 kHz horizontally and 10 dB/cm vertically. The analyzer bandwidth per resolution cell is about 4 Hz. The modulating signal is seen at about 1.5 kHz at a level about 40 dB above the noise floor. The other spectral lines evident in the data are caused by acoustic sensing of ambient room noises generated by test equipment fans, air conditioning, etc.

This demonstrated signal-to-noise ratio implies the ability to sense peak phase modulations of  $4 \times 10^{-4}$  radians corresponding to about 0.14 Angstroms RMS displacement in the 4 Hz bandwidth, which is half of this normalized to a 1 Hz bandwidth. In obtaining this data, no efforts were made to realize good noise performance and the results are far from photon noise limited. Thus, considerable improvement is potentially available by improving the noise characteristics of the photodetector and preamplifier. Recall from an earlier discussion that  $4 \times 10^{-7}$  radians are potentially realizable at practical light levels.

A coiled optical fiber is another acoustic sensor which was briefly used in this system. When subjected to uniform pressure, an optical fiber changes its optical transit delay due to a combination of density and mechanical length changes. Coiled lengths of such fibers have been used as optical hydrophones by sensing their acoustically induced phase delay modulations [2].

About 10 meters of fiber were wound into a 4 cm diameter coil and spliced to fiber leads with intentionally misregistered cores at the splices. The misregistration was intended to generate the required partially reflecting boundaries. Even though the misregistrations caused severe light leakage at the splices, the reflections it produced were too weak to be visually detected. By comparison, the 4 percent reflections from the gap hydrophone discussed above had been readily visible.

Furthermore, fiber losses through this short length and large bending radius coil were small, implying too large an  $\xi$  according to Figure 3. The high light levels available at the photodetectors were also arbitrarily attenuated as a convenience to prevent saturation. In spite of all these non-optimal conditions, the fiber worked well as an acoustic sensor.

Figure 8a shows the IF spectrum from 0 to 20 kHz at 10 dB/cm. The sideband is 13 dB below the carrier implying 0.3 radians RMS phase modulation.

Figure 8b is the demodulated spectrum from 0 to 10 kHz at 10 dB/cm. The demodulated signal at 5 kHz is seen to be about 32 dB above the noise floor, implying a minimum detectable RMS phase modulation of about 0.008 radians. Figure 8c shows the demodulated time waveform.

### Summary

Optical fiber data transmission lines combined with acoustic sensors that directly modulate the light in the fibers offer the possibility of dramatic reductions in the size, weight, and cost of low frequency sonar sensor arrays. A practical problem in such systems is distinguishing the desired modulation imposed at the sensor location from undesired extraneous modulations accumulated along the entire fiber lead length. A system is presented which solves this problem. It uses a pair of single-mode optical fibers connected to each sensor. The boundaries between the sensing element and the fiber leads are delineated by partially reflecting optical discontinuities. The sensing element can be any device capable of optically coupling the two fibers together with an optical transit time delay that is affected by acoustic vibrations.

An acoustically driven gap between the planar end faces of the two lead fibers, and a coiled optical fiber are examples of two suitable sensors that have been experimentally demonstrated in this system. Using available test equipment that has not been optimized for good noise performance, a sensitivity equivalent to  $2 \times 10^{-4}$  radians RMS phase modulation in a 1 Hz bandwidth has been demonstrated. Making conservative estimates about pertinent system parameters implies a sensitivity of about  $4 \times 10^{-7}$  radians RMS phase modulation in a 1 Hz bandwidth, if photon noise limited performance can be approached. The relationship between phase modulation and acoustic level depends on the acousto-optic mechanical properties of the sensing element, which are subject to the details of the hydrophone design. Using the gap hydrophone as implemented, demonstrated sensitivity is approaching useful levels at low frequencies and projected sensitivity is well beyond that needed to sense background acoustic noise in a quiet sea.

### References

- [1] Electronics Engineers' Handbook, D. Fink, Editor in Chief, McGraw-Hill Book Co., 1975, Section 3-30
- [2] "Fiber-optic Hydrophone," J. Bucaro and D. Darby, J. Acoustic Soc. Am., Vol. 62, No. 5, Nov. 1977, pg. 1302-1138.

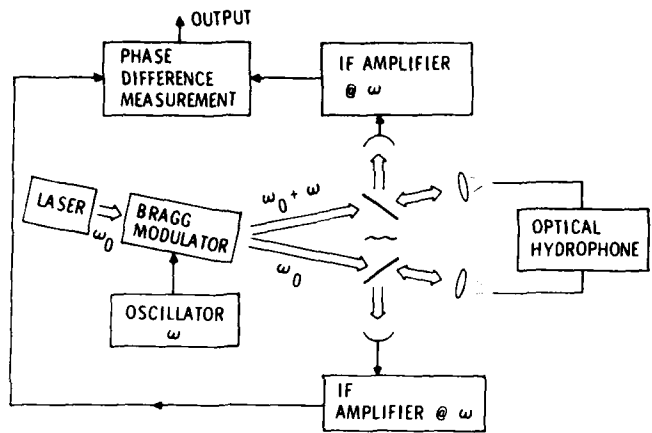


Figure 1. Optical Heterodyne Hydrophone System

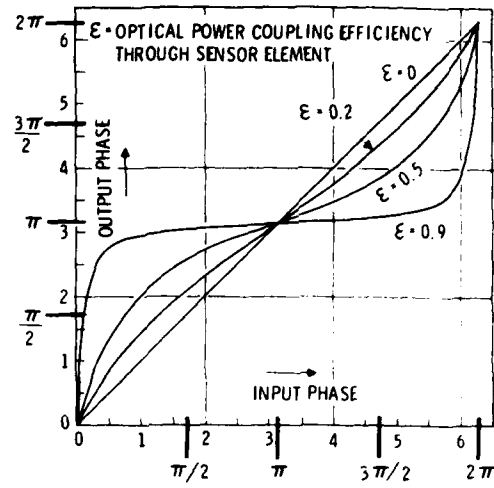


Figure 3. Output Phase vs. Input Phase Delay Through Sensor

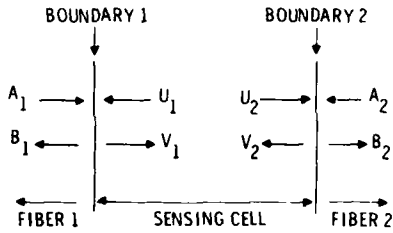


Figure 2. Complex Light Amplitudes at Sensor Boundaries

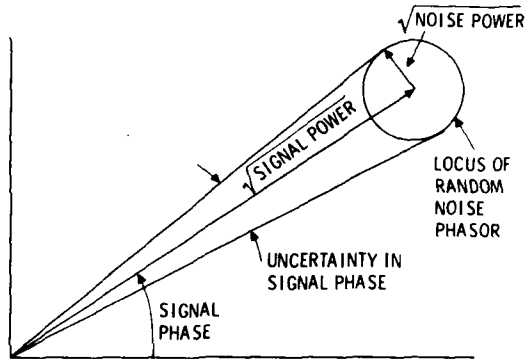


Figure 5. Phase Uncertainty Due to Additive Noise

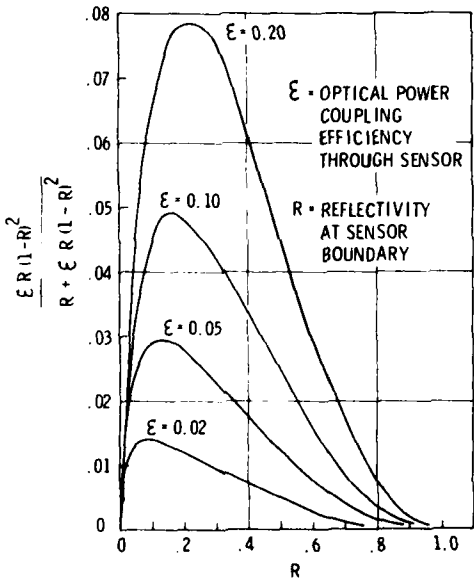


Figure 4. Optimum Reflectivity

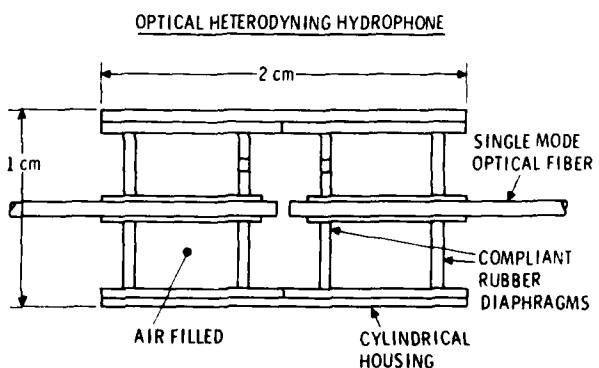
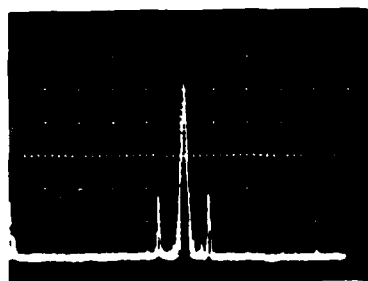


Figure 6. Optical Heterodyning Hydrophone



IF SPECTRUM

0 → 20 KHz

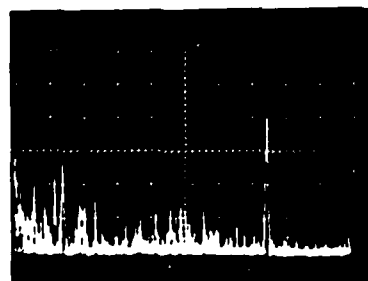
10 dB/cm

$$20 \log \left[ \frac{J_0(4\pi X \lambda)}{J_1(4\pi X \lambda)} \right] = 34 \text{ dB}$$

$$J_0(4\pi X \lambda) = 50 J_1(4\pi X \lambda)$$

$$4\pi X \lambda = 0.04 \quad \lambda = 6328 \text{ Å}$$

$$X = 20 \text{ Å} \quad X \sqrt{2} = 14 \text{ Å}$$



FM DEMODULATED SPECTRUM

0 → 2 KHz

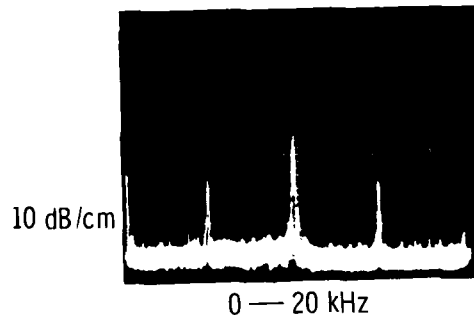
10 dB/cm

S/N ≈ 40 dB

$$X \sqrt{2} / \lambda_{\text{air}} \approx 0.14 \text{ Å}$$

Figure 7a. IF Spectrum From Gap Hydrophone

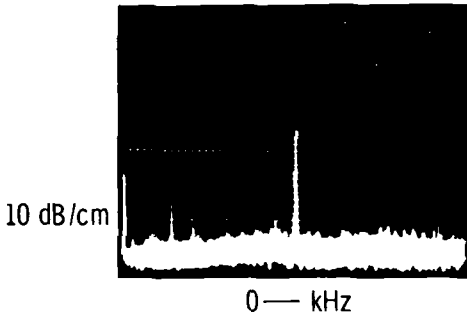
Figure 7b. Demodulated Spectrum From Gap Hydrophone



10 dB/cm

0 → 20 KHz

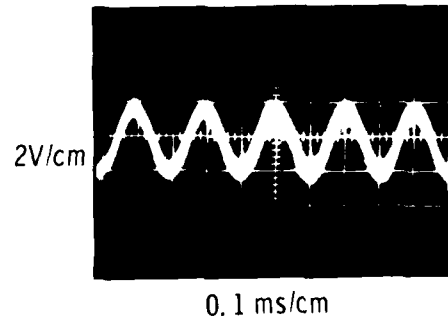
Figure 8a. IF Spectrum



10 dB/cm

0 → kHz

Figure 8b. Demodulated Spectrum



2V/cm

0.1 ms/cm

Figure 8c. Time Waveform

#### COILED HYDROPHONE WITH 5-kHz DRIVE

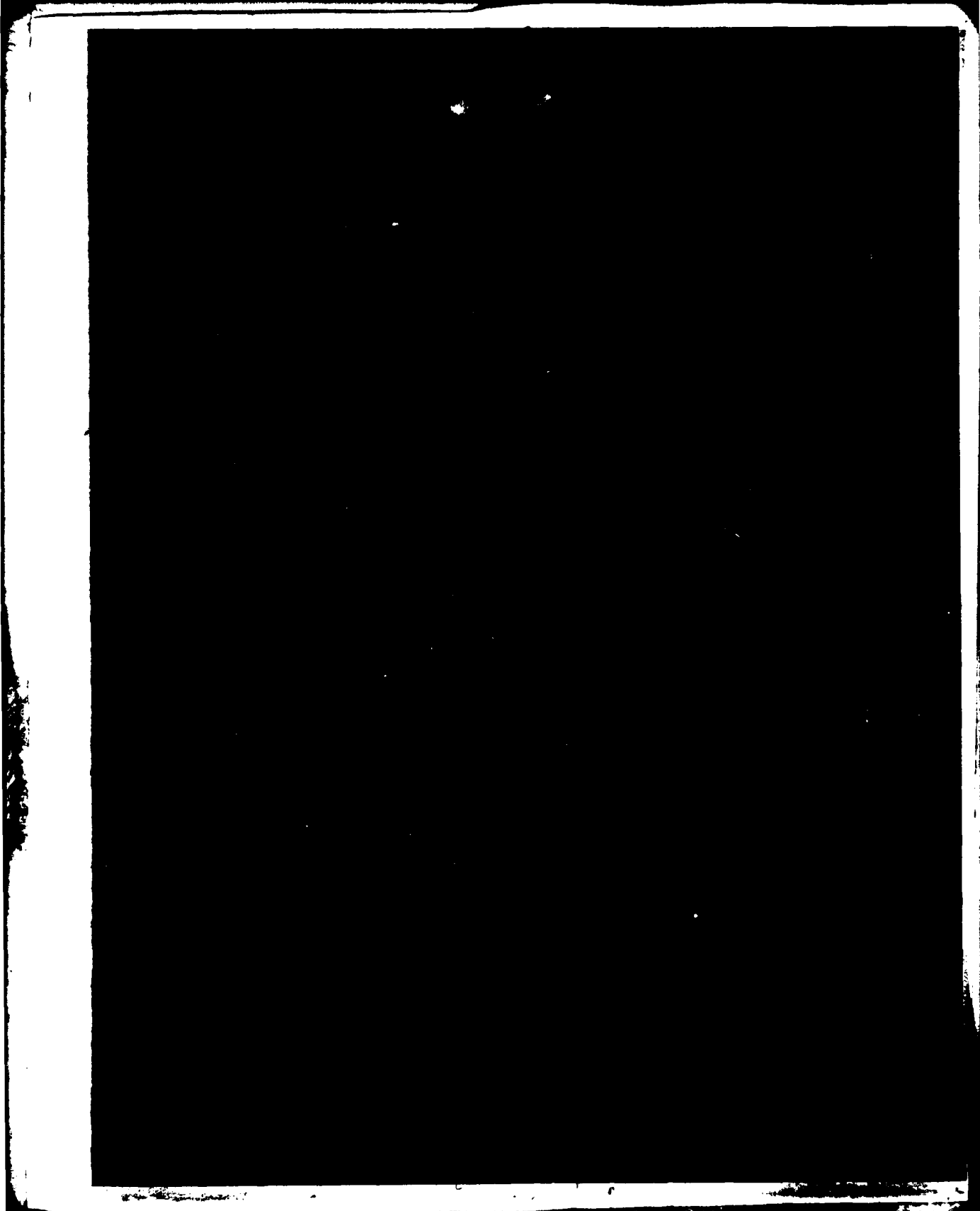
$$20 \log \frac{J_0(\phi)}{J_1(\phi)} = 13 \text{ dB}$$

$$J_0(\phi) = 4.47 J_1(\phi)$$

$$\phi = 0.437 \text{ RADIANS} \quad \phi / \sqrt{2} = 0.309 \text{ RADIANS}$$

$$S/N \cong 32 \text{ dB} = 39.8$$

$$(\phi / \sqrt{2})_{\text{MIN}} \cong 0.00776 \text{ RADIANS}$$



FILME

